ARTICLE

Glass formation and dynamics of model polymer films with one versus two active interfaces

Received 00th January 20xx, Accepted 00th January 20xx

DOI: 10.1039/x0xx00000x

Asieh Ghanekarade^a and David S. Simmons^{*a}

Polymers and other glass-forming liquids can exhibit profound alterations in dynamics in the nanoscale vicinity of interfaces, over a range appreciably exceeding that of typical interfacial thermodynamic gradients. The understanding of these dynamical gradients is particularly complicated in systems with internal or external nanoscale dimensions, where a gradient nucleated at one interface can impinge on a second, potentially distinct, interface. To better understand the interactions that govern system dynamics and glass formation in these cases, here we simulate the baseline case of a glass-forming polymer film, over a wide range of thickness, supported on a dynamically neutral substrate that has little effect on nearby dynamics. We compare these results to our prior simulations of freestanding films. Results indicate that dynamical gradients in our simulated systems, as measured based upon translational relaxation, are simply truncated when they impinge on a secondary surface that is locally dynamically neutral. Altered film behavior can be described almost entirely by gradient effects down to the thinnest films probed, with no evidence for finite-size effects sometimes posited to play a role in these systems. Finally, our simulations predict that linear gradient overlap effects in the presence of symmetric dynamically active interfaces yield a non-monotonic variation of the whole free standing film stretching exponent (relaxation time distribution breadth). The maximum relaxation time distribution breadth in simulation is found at a film thickness of 4-5 times the interfacial gradient range. Observation of this maximum in experiment would provide an important validation that the gradient behavior observed in simulation persists to experimental timescales. If validated, observation of this maximum would potentially also enable determination of the dynamic gradient range from experimental mean-film measurements of film dynamics.

Introduction

Across a wide range of glass-forming liquids possessing structure or dimensions on the sub-100 nm scale, confinement and proximity to interfaces can dramatically alter dynamics and the glass transition temperature $T_g.^{1-12}$ The nature of the interface(s) in these systems - whether free, soft or rigid, and whether attractive or repulsive - plays a central role in mediating their magnitude and even direction ^{13–21}. Over the last decade, a reasonably cohesive picture of the nature of equilibrium dynamical gradients at single interfaces of thick domains has begun to emerge for many of these systems.8 However, real nano-dimensioned and nanostructured materials and fluids commonly possess domain sizes sufficiently small that alterations imposed by distinct interfaces can interact. These situations can range from symmetrical cases, such as a freestanding film, in which all interfaces involved are of the same type, to highly asymmetrical cases such as films supported on rigid attractive substrates, to even more complex cases such as nanocomposite thin films involving a free surface, a substrate, and a particle interface. In cases such as these, resolving the extent to which dynamical alterations are

attributable to each interface, and understanding the interplay between alterations emanating from each interface, is a durable challenge of both fundamental and practical importance.

The most extensive understanding of shifts in dynamics in the thick-domain, single-interface limit is presently available near free surfaces8. Here, altered equilibrium dynamics take the form of a large interfacial gradient of accelerated dynamics at the free surface, which is characterized by an exponential recovery of bulk-like activation barriers with increasing distance from the surface, over at least the first ~10 segmental diameters from the surface²². Consistently with this, bulk-like segmental relaxation times are recovered in a double-exponential $\label{eq:gradient} \mbox{gradient}^{22\mbox{-}28} \mbox{ with increasing distance from the surface over this}$ range, with a corresponding exponential T_g gradient^{25,29–31}. Beyond about 10 segmental diameters, a likely inverse power law gradient tail extends much further into the film³². A recent experimental study probing surface diffusion as a function of the penetration depth of surface molecules across a range of liquids supports the near-surface double-exponential decay²⁷. The temperature dependence of this gradient is now fairly well understood as well: at low enough temperatures, the fractional reduction in activation barrier relative to bulk is nearly temperature invariant at any given distance from the surface, leading to a fractional power law relation between local, film, and bulk relaxation times^{8,22,33–36}.

^a Department of Chemical, Biological, and Materials Engineering, The University of South Florida, Tampa, Florida.

b. Address correspondence to dssimmons@usf.edu

Recently, we probed in simulation the question of how this picture is altered in a freestanding film for which the two free surfaces are sufficiently close as to allow their corresponding dynamical gradients to interact³⁶. We found that for most conditions the overall effect could be described to leading order based on an assumption of linear additivity of the activation barrier gradients emanating from the two interfaces. Some second order corrections to this additivity were observed for intermediate films and attributed there to potential elasticityrelated finite size effects; more recent work suggests that a more precise description may be that these deviations result from additivity of a low-magnitude elasticity-driven power law gradient tail found beyond the first ~10 nm from the surface³². Stronger deviations from gradient additivity were found in ultrathin films, where the overall suppression of elastic contributions to the activation barrier saturates such that little to no more reduction of this barrier contribution is possible as thickness is further reduced³⁶.

Earlier simulation evidence from Hsu et al. suggested that this leading-order gradient additivity scenario may extend to a broader array of systems involving distinct types of interfaces 31 . There, they argued that simulations of both freestanding films (where T_g decreases at both surfaces) and films supported on rigid attractive substrates (where T_g increases at the substrate but decreases at the free surface) could be described to leading order by a simple summation of the T_g gradients emanating from the two interfaces. This suggests a simple and generalizable scenario for how to infer mean-system T_g shifts in systems involving multiple interface types.

Despite this progress, serious complexities remain in understanding altered dynamics in thin films with distinct interface types, particularly in the ultra-thin film limit. For example, when a dynamical gradient emanating from a free surface encounters a substrate, how is it altered? Is it merely truncated, or is the effect more complex? Do the second-order deviations from exponential gradient additivity we recently reported in freestanding films play a role in ultra-thin supported films? Is there any evidence in simulation for nontrivial interactions between the two interfaces such as recently been suggested based on experiments probing these types of systems?^{37,38}. How is the breadth of the glass transition and relaxation spectrum impacted in these cases?

To begin answering these questions, we perform simulations of the simplest possible asymmetric film: a film supported on a dynamically neutral substrate that does not significantly perturb local dynamics. We compare the results of these simulations to our prior simulations of freestanding films employing a similar model. In the simple neutrally-supported film case, one can directly assess the outcome when a freesurface-nucleated dynamical gradient impinges on a substrate, in the absence of a confounding second gradient. One can test for the presence of non-additive finite size effects readily, since no gradient additivity is possible in the absence of a second gradient. This system also provides an excellent baseline for

understanding the effect of gradient additivity on the breadth of relaxation processes.

Our results suggest that the model of gradient additivity (linear gradient superposition) is remarkably predictive, to leading order. We find that a dynamically neutral substrate has little effect on the free surface gradient, serving to leading order simply as a truncating plane for the gradient. This implies that the 'steepness' of the gradient is essentially innately thickness independent, although gradient additivity effects can lead to flattening in the presence of multiple dynamically active gradients for mathematical reasons. As a result of this phenomenon, our simulations predict a fascinating nonmonotonic thickness dependence of the breadth of the relaxation spectrum in freestanding films but not in neutrally supported films. Observation of this behaviour in future experiments could provide valuable support validating the persistence of this simulated behaviour to experimental timescales, while also potentially providing experimental insight into the dynamical gradient range in experimental nanostructured systems.

Methodology

We perform simulations of bead-spring polymer films supported on a dynamically neutral substrate, over a broad range of film thicknesses. Simulations employ a modified version of the attractive bead-spring model based on the work of Kremer and Grest³⁹, with each chain comprised of 20 beads. Nonbonded beads of species *i* and *j* interact via the 12-6 Lennard Jones potential,

$$E_{ij} = 4\varepsilon \left[\sigma^{12} r^{-12} - \sigma^6 r^{-6} \right]. \tag{1}$$

Interactions between polymer beads employ ϵ and σ both equal to 1 and with interactions cut off at a distance of 2.5; substrate interactions are discussed below. Bonded beads interact via the Finitely Extensible Nonlinear Elastic (FENE) potential combined with a binary LJ potential,

$$E_{bond} = -0.5KR_0^2\ln\left(1-r^2R_0^{-2}\right) + 4\varepsilon_{bond}\left[\sigma_{bond}^{-12}r^{-12} - \sigma_{bond}^{-6}r^{-6}\right], (2)$$

with K=30, $\varepsilon_{bond}=1.0$, $R_0=1.3$, and $\sigma_{bond}=0.8$; the latter two of these are modified from their most common values to yield improved crystallization resistance while in contact with a solid substrate⁴⁰. We note that this model differs slightly from the one employed in our recent freestanding film simulations, to which we compare our new results. However, both models lie within a range of bead-spring polymer backbone bond lengths that we have previously shown to exhibit essentially invariant response to nanoconfinement⁴¹, such that their results are expected to be closely comparable.

Simulations of both supported film and bulk reference systems were performed in the LAMMPS molecular simulation package⁴². Temperature selection and simulation time selection for bulk systems are automated via the Predictive Stepwise Quench (PreSQ) algorithm described in our prior work⁴³; supported thin film

simulations are then performed at the same set of temperatures as bulk to enable isothermal comparison between film and bulk. The bulk system is simulated at pressure P = 0 by employing the Nose-Hoover thermostat and barostat as implemented in LAMMPS, with pressure and temperature damping parameters of 2 τ_{\square} (where τ_{\square} is the LJ unit of time and is approximately equal to a picosecond in real units). Film simulations are nominally performed at constant volume, but the presence of a free surface yields an effectively constant pressure P = 0 boundary condition for the film itself.

The substrate consists of LJ beads arranged on an FCC lattice at a number density of 1.4, with the [111] face exposed to the fluid. We arrive at a dynamically neutral substrate by tuning the polymer-substrate interaction energy parameter ϵ_{ps} until dynamics are essential unperturbed near the substrate. As shown in our recent paper 32 , a value of ϵ_{ps} = 0.515 yields a negligible dynamical gradient at the substrate, and we confirm in the results section that this yields a negligible T_g gradient near the substrate.

We simulate these supported film systems over a range of film thickness ranging from 3 σ_{LJ} to 49 σ_{LJ} thick, where σ_{LJ} is the LJ unit of length and corresponds to approximately a nanometer in real units^{3,39,44}. The film thickness is naturally temperature dependent, reflecting the density equation of state of the system; we employ a reduced temperature T = 0.5 as our reference temperature for designation of a nominal thickness. The cross-sectional area of the simulation is 23 σ_{LJ} x 20 σ_{LJ} in all cases except the 49 σ_{LJ} thick film, for which the cross-sectional area is 41.7 σ_{LJ} x 40 σ_{LJ} .

In quantifying the dynamics of these systems, we focus on translational dynamics as computed from the self-intermediate scattering function:

$$F_{s}(\boldsymbol{q},t) = \frac{1}{N} \sum_{j}^{N} \left\langle \exp\left[-i\boldsymbol{q} \cdot \left(\boldsymbol{r}_{j}(t) - \boldsymbol{r}_{j}(0)\right)\right]\right\rangle.$$
(3)

Here ${\it q}$ is the wavevector, ${\it r}_i$ is the position of bead i, and t is time. We compute the value of this function at a wavenumber q = 7.07 (comparable to the first peak of the structure factor) by averaging in a radially symmetric manner over multiple wavevectors with magnitudes in a narrow band around this wavenumber, as is standard for many studies probing dynamics near various interfaces including free surfaces and rigid substrates and particles including free surfaces and rigid substrates and particles 20,21,29,32,45,46 . A relaxation time and stretching exponent are extracted by fitting $F_s(q,t)$ to the Kohlraush-Williams-Watt (KWW) stretched exponential function, 47,48

$$F_{s}(q,t) = A \exp\left[-\left(t/\tau_{KWW}\right)^{\beta}\right] \tag{4}$$

and then defining the alpha relaxation time τ to be the time at which this function is equal to 0.2, a commonly used convention in the simulation literature^{29,31,46,49,50}. We perform this fit only over the domain for which $F_s(q,t) \leq 0.6$ in order to optimize the fit to the alpha relaxation process specifically and exclude earlier features of the relaxation process.

We then extract glass transition temperatures $T_{\rm g}$ from data of this kind obtained over multiple temperatures. To do so, we fit

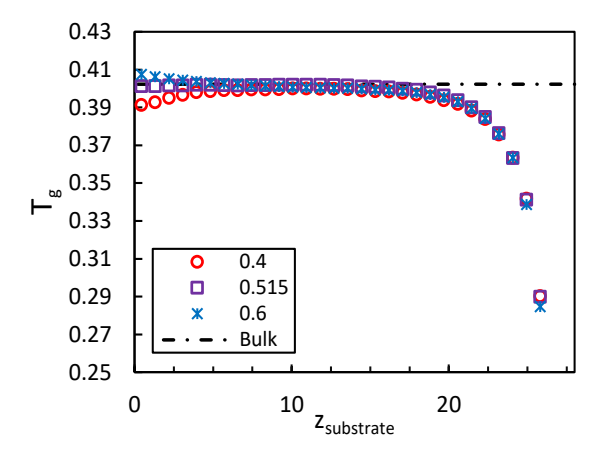


Figure 1 - Glass transition temperatures versus z at $\epsilon_{polymer.substrate}$ values of 0.4 (red circles), 0.515 (purple squares), and 0.6 (blue stars).

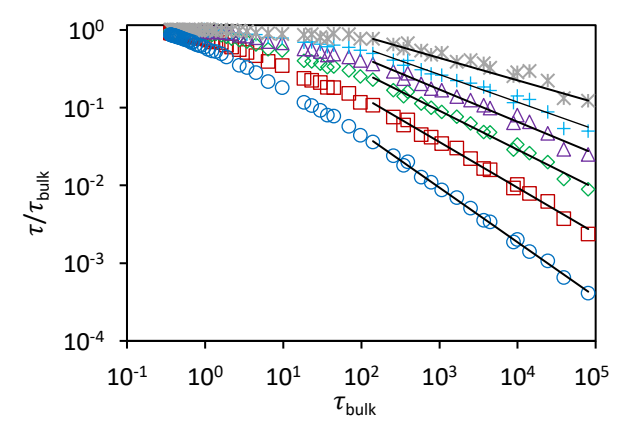


Figure 2 - Segmental relaxation time versus bulk relaxation time for a film of thickness 17 σ_{IJ} , for layers of segments at distances z from the surface of 0.4375 σ (blue circles), 1.3125 σ_{IJ} (red squares), 2.1875 σ_{IJ} (green diamonds), 3.0625 σ_{IJ} (purple triangles), 3.9375 σ_{IJ} (blue pluses), and 4.8125 σ_{IJ} (gray stars). Lines are fits of the long-time data to equation (5).

these data to the Vogel-Fulcher-Tammann relation 51,52 , and we define T_g on a computational timescale as the temperature at which the relaxation time first exceeds $10^5\,\tau_{lj}$. We perform all of the analysis above at a spatially resolved level by first binning the particles based upon their distance (in \Box distance units of σ_{\Box} , approximately equal to nm) from the substrate or free surface and then computing local dynamical properties of particles within each bin.

Results and Discussion

Dynamical gradients

We begin by confirming that the polymer-substrate interaction we employ indeed yields an approximately dynamically neutral substrate. In Figure 1, we report the gradient of T_g as a function of distance from the substrate for the neutral value employed in the study ($\epsilon_{ps}=0.515$) and for two other bracketing values of the substrate-polymer interaction. As can be seen here, alterations in T_g at the substrate are weak, at most, for $\epsilon_{ps}=0.515$, with a slight near-substrate suppression observable. This outcome makes use of the concept of a 'compensation point' of

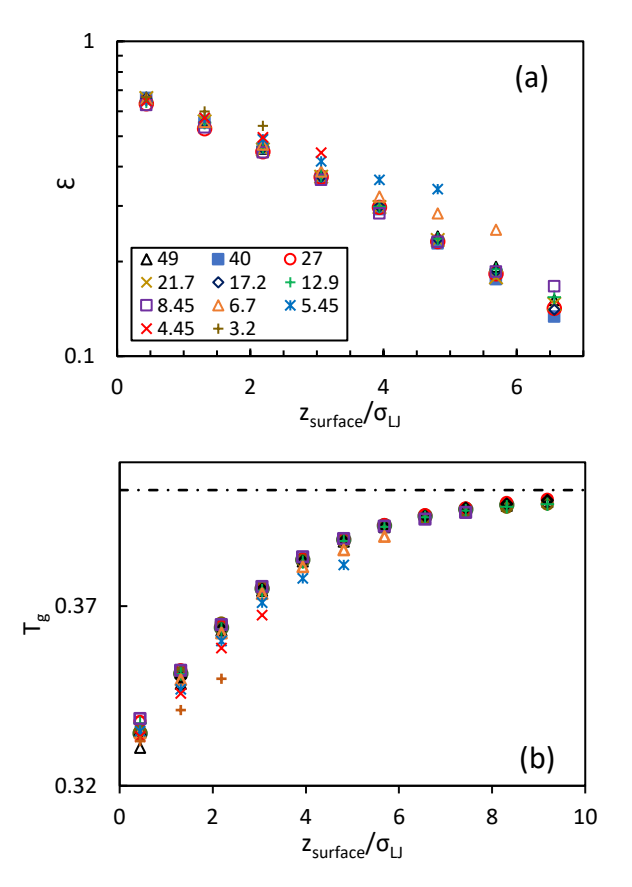


Figure 3. (a) Effective barrier reduction ratio ϵ and (b) glass transition temperature near the film surface as a function of distance from the surface, for films of total thickness $49\sigma_{\text{Ll}}$ (black triangles), $40~\sigma_{\text{Ll}}$ (filled blue squares), $27\sigma_{\text{Ll}}$ (red circles), $21.7\sigma_{\text{Ll}}$ (brown x's), $17.2\sigma_{\text{Ll}}$ (black diamonds), $12.9\sigma_{\text{Ll}}$ (green pluses), $8.45\sigma_{\text{Ll}}$ (purple squares), $6.7\sigma_{\text{Ll}}$ (orange triangles), $5.45\sigma_{\text{Ll}}$ (blue stars), $4.45\sigma_{\text{Ll}}$ (red x's), $3.2\sigma_{\text{Ll}}$ (brown pluses)

interfacial interaction at which alterations in dynamics are absent; notably, this condition is quite distinct from that of thermodynamic neutrality^{16,20,53}. We note that in arriving at this value we found that it is not possible to achieve perfect neutrality at all temperatures because the dynamic neutrality condition is slightly temperature dependent, but the substrate effect here is sufficiently weak as to require only minor corrections in the data analysis, as discussed below. It is also probable that this neutrality condition averages over a degree of anisotropic dynamics near the substrate, but prior studies have indicated that any near-substrate anisotropy in dynamics is extremely short ranged – much shorter than the range of the dynamical gradient itself²⁹. We emphasize that, as described in the methods, we compute a radially averaged measure of translational relaxation such that this neutrality condition averages over the in- and out-of-plane components of any such short-ranged anisotropy.

In analysing more deeply the local dynamics in these systems, we make use of a fractional power law decoupling relation between local and bulk dynamics that was discovered in our prior work²² and has since been observed in a number of additional systems^{33,35,36,54} and predicted theoretically^{33,36,55}. As a consequence of this relation, which is predicted and observed

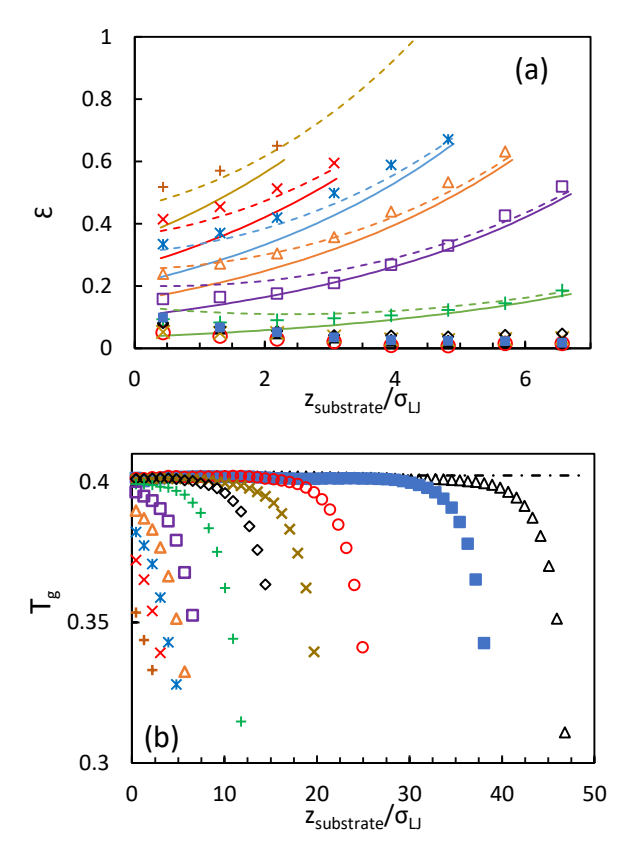


Figure 4 - (a) Effective barrier reduction ratio ϵ and (b) glass transition temperature, as a function of distance from the substrate, for films of thickness $49\sigma_{Ll}$ (black triangles), $40\sigma_{Ll}$ (filled blue squares), $27\sigma_{Ll}$ (red circles), $21.7\sigma_{Ll}$ (brown x's), $17.2\sigma_{Ll}$ (black diamonds), $12.9\sigma_{Ll}$ (green pluses), $8.45\sigma_{Ll}$ (purple squares), $6.7\sigma_{Ll}$ (orange triangles), $5.45\sigma_{Ll}$ (blue stars), $4.45\sigma_{Ll}$ (red x's), $3.2\sigma_{Ll}$ (brown pluses). The solid lines in part (a) report on the behaviour predicted based on a scenario wherein the thick-film free surface gradient (equation (7) with A = 0.75 and ξ = 4.3 σ) is simply truncated at the substrate. The dashed lines represent the combination of the thick film surface and (much weaker) substrate gradients as per equation (9). In both cases predictions are made for h consistent with the data set in matching color.

to hold at low temperature, local dynamics near a surface are related to the bulk dynamics via the relation

$$\frac{\tau(T,z)}{\tau_{bulk}(T)} = \left(\frac{\tau_{bulk}(T)}{\tau^*}\right)^{-\varepsilon(z)}$$
 (5)

where τ^* specifies an onset condition for this behaviour on cooling and ε is called the "decoupling parameter". Combining this observation with a generalized activation rule possessing a temperature-dependent activation barrier leads to the conclusion that the decoupling exponent reports on the local fractional reduction in the local activation barrier $\Delta F(T,z)$ relative to the bulk activation barrier $\Delta F_{bulk}(T)$:8,22,55

$$\varepsilon(z) = 1 - \frac{\Delta F(T, z)}{\Delta F_{bulk}(T)} \tag{6}$$

As shown in Figure 2, equation (5) and thus equation (6) indeed hold locally when temperatures are sufficiently low for a representative film of thickness 17 σ_{LL} .

On this basis, we employ equation (5) to extract the relative reduction in activation barrier within the film as a function of distance from the free surface. As shown in Figure 2, we perform this fit including temperatures for which $\tau_{bulk} > 10^2 \, \tau_{LJ}$. This temperature range is chosen to be below the approximate onset timescale of this behaviour (i.e. we fit the long-timescale range of behaviour for which the data are actually linear in this plot). As shown in Figure 3a, the activation barrier truncation gradient near the free surface closely obeys an exponential decay form with increasing depth in the film, consistent with prior work^{22,35,36}:

$$\varepsilon(z_{surf}) = \varepsilon_{0,surf} \exp(-z_{surf}/\xi_{\Delta F,surf}). \tag{7}$$

Here z_{surf} is the distance from the free surface, and we find a good fit to thick film surface gradient data with prefactor $\epsilon_{0,surf}$ = 0.75 and exponential decay range $\xi_{\Delta F,surf}$ = 4.3 σ_{LJ} . In our prior work in freestanding films, substantial deviations from this form were observed for films of thickness h \leq 15 σ_{LJ} , as a consequence of large gradient overlap effects. Here, however, the single-exponential gradient form remains quantitative down to a film of only $8\sigma_{LJ}$ in thickness, and deviations from this form remain mild even for the thinnest films. A similar trend is seen in Figure 3b for T_g gradients: the exponential T_g gradient behaviour observed for thick films remains reasonably descriptive of the gradient even for quite thin films.

In Figure 4, we consider the implications of this behaviour for dynamics near the substrate. As can be seen here, for thick films the activation barrier and T_g near the substrate are only weakly perturbed from bulk. Indeed, as seen in Figure 4a, in the thick film limit ϵ is only slightly enhanced near the substrate, and we find that this can again be fit with an exponential gradient near the substrate,

$$\varepsilon(z_{sub}) = \varepsilon_{0,sub} \exp(-z_{sub}/\xi_{\Delta F,sub}), \qquad (8)$$

where z_{sub} is the distance from the substrate, and where we find that the substrate gradient is of much smaller magnitude, with $\varepsilon_{0,sub}$ = 0.10 and $\xi_{\Delta F,sub}$ = 3.1 $\sigma_{\rm LJ}$.

With decreasing film thickness, the near-substrate dynamics become quite accelerated, but this trend is driven by the surface effect impinging on the substrate rather than by an emergent substrate effect. Indeed, we can confirm this origin by comparing this enhancement to expectations from the thick-film interfacial gradient measurements. The solid lines in Figure 4a report on the behaviour that would be expected if only the exponential free surface gradient (i.e. equation (7)) were present and were simply truncated at the substrate, obtained by combining equation (7) with the identity that $z_{sub} = h - z_{surf}$. As can be seen, this provides a good description of the data down to h = 8.5 except very near the substrate, but somewhat underpredicts the barrier truncation for thinner films. A better prediction of the thin film data can be obtained by simply summing the two barrier gradients, as

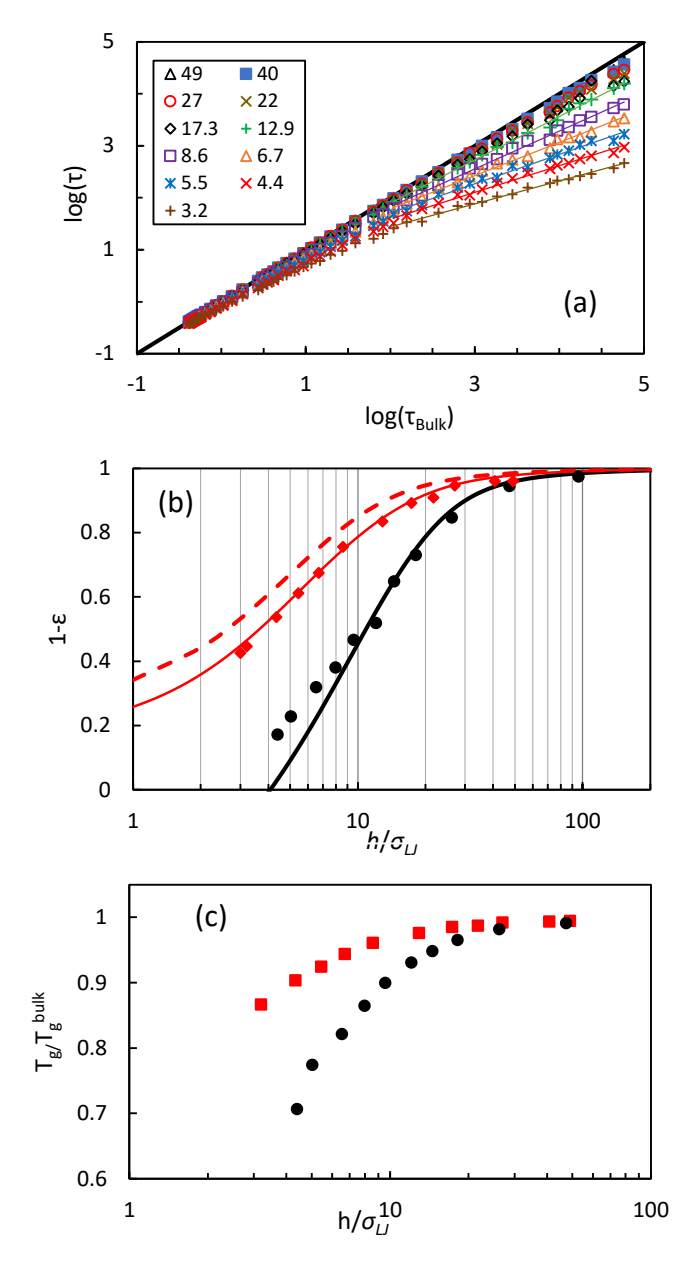


Figure 5 - (a) Mean film relaxation time versus bulk relaxation time for films of thickness $49\sigma_{\sqcup}$ (black triangles), $40~\sigma_{\sqcup}$ (filled blue squares), $27\sigma_{\sqcup}$ (red circles), $21.7\sigma_{\sqcup}$ (brown x's), $17.2~\sigma_{\sqcup}$ (black diamonds), $12.9\sigma_{\sqcup}$ (green pluses), $8.45\sigma_{\sqcup}$ (purple squares), $6.7\sigma_{\sqcup}$ (orange triangles), $5.45\sigma_{\sqcup}$ (blue stars), $4.45\sigma_{\sqcup}$ (red x's), $3.2\sigma_{\sqcup}$ (brown pluses). Solid lines are linear fits to the low-temperature data indicating the low-temperature fit to the fractional power law decoupling relation at a whole-film level. (b) Fraction of bulk barrier remaining (i.e. $1\text{-}\epsilon(h)$) vs film thickness. Black circles and red diamonds are simulation data for freestanding and neutrally supported films, respectively. The black curve is the prediction of linear gradient additivity for the freestanding film. The red dashed curve is the prediction of an idealized surface gradient truncation effect at the dynamically neutral substrate. The solid red curve is the prediction of gradient additivity for the neutrally-supported film, taking into account the near-negligible substrate gradient. (c) Film Tg normalized by the corresponding bulk value, plotted vs film thickness, for the neutrally supported film (red squares) and the freestanding film (black circles).

$$\varepsilon(z_{sub}) = \varepsilon_{0,sub} \exp(-z_{sub}/\xi_{\Delta F,sub}) + \varepsilon_{0,surf} \exp(-(h-z_{\Delta F,surf})/\xi_{\Delta F,surf})$$
(9)

As shown by the dashed lines in Figure 4a, this model of simple superposition of the two exponential barrier suppression gradients provides good predictions over the first 6-7 σ_{LJ} near the substrate for films over the entire range of thickness. This indicates that the near-dynamically-neutral substrate behaviour designed in the thick-film limit remains near-neutral down to very thin films. The accelerated near-substrate dynamics seen in very thin films is thus the consequence of the free-surface-nucleated dynamical gradient extending to the substrate to an appreciable degree once $h < 2\xi_{\Delta F, surf}.$

Combined with Figure 3, this indicates that the dynamically neutral substrate simply truncates the surface-induced gradient to leading order (to within the weak residual substrate effect) rather than altering it. Unlike in freestanding films, where additivity of two strong surface gradients leads to flattening of the combined gradient in very thin films³⁶, here this effect is absent. The gradient remains essentially equivalently steep for all film thicknesses. This indicates that a dynamically neutral substrate does not serve to 'pin' the local dynamics to their bulk rate, but simply has no impact upon near-substrate dynamics at all, to leading order.

Thickness-dependence of mean-film activation barrier and $T_{\rm g}$

We now turn to the question of the mean behaviour of our simulated film and its dependence on film thickness in the ultrathin-film limit. This type of data is more typically the subject of experimental studies. Experimental data of this kind have been shown to be accessible for both mean film T_g and mean film effective activation barriers 37,38 , and we thus aim to understand the thickness-variation of both.

As can be seen in Figure 5a, whole-film dynamics for the systems simulated here also obey the fractional power law decoupling relation, with film dynamics progressively accelerating as thickness is reduced. As with the analysis of local dynamics, we can extract the value of $\varepsilon(h)$ by fitting the data to equation (5), with z replaced by the film thickness h, for data for which $\tau_b > 10^2$. As shown in Figure 5b, $\varepsilon(h)$ exhibits a progressive reduction with decreasing film thickness. How does this whole-film behaviour compare to that observed in a freestanding film?

As shown in Figure 5b, the drop in activation barrier with reducing film thickness for the neutrally-supported film is considerably weaker than for the freestanding film. This is a consequence of the lack of a strong second additive dynamical gradient in the supported film, which was present in the freestanding film.

In order to quantitatively model the mean behaviour of this film, we describe the surface activation barrier gradient as exponential as indicated by equation (7). We then average over the film, truncating the gradient at the substrate, and employing the correct weighting function for averaging of the local activation barrier gradient established in our prior work³⁶.

As can be seen in Figure 5b, the resulting dependence of the predicted mean-film qualitatively captures the variation of the data with film thickness, but slightly underpredicts the reduction in activation barrier. This underprediction is a consequence of a slight residual gradient at the substrate, as is described above can be seen in Figure 1. Accounting for this weak substrate gradient within the film average leads to a nearly exact quantitative prediction of the thickness-variation of the mean-film activation barrier from the thick-film gradients, as can be seen in Figure 5b.

Indeed, the quality of prediction obtained by simply averaging over the exponential gradient is appreciably better for the supported film than for a freestanding film. As discussed in our prior work, there are appreciable downward deviations (for intermediate thickness films) and upward deviations (for ultrathin films) from the two-exponential-gradient superposition model in the case of freestanding films. This is a consequence of the overlap of long-range elastic power-law tails in the intermediate film³², and of a saturation of elastic effects from two interfaces in ultra-thin films³⁶.

Evidently, these two-interface effects are relatively weak when one of the two interfaces is dynamically neutral. There is perhaps a suggestion in Figure 5b of a slight underprediction of the amount of barrier truncation in intermediate-thickness supported films: for nearly all of our thicker films the red curve is slightly above the datapoints. This underprediction is likely a consequence of omitting the recently-discovered power-law gradient tail³². from our mean-film average. However, the effect is relatively weak as compared to the freestanding film, which involves two additive power law tails in intermediate thickness films. We emphasize that this power-law tail is not a finite size effect; rather it is simply a long-ranged component of the gradient. At the same time, there is no indication of an overprediction of barrier truncation in the thinnest supported films, in contrast to the freestanding film. In the freestanding film, this was a consequence of a saturation of truncated elastic barriers. The elastic barrier to activation is essentially already zeroed out for some finite thickness freestanding films, such that a naïve gradient additivity model overpredicts the barrier truncation in the thinnest films. This again is not best understood as a true finite size effect, but merely a saturation of the gradient effect. This effect is absent in supported films, because the amount of elastic activation barrier reduction is effectively halved in the thinnest films in the absence of a second interface. This suggests that there are no true finite size effects present in this system at a level detectable in mean-film dynamics, since any such effect should be present as a result of length-scale truncation even in the presence of a dynamically neutral interface.

Moving now to mean-film T_g behavior, as shown by Figure 5c, T_g exhibits a progressive suppression with decreasing film thickness, in a manner qualitatively consistent with experiment^{38,56}. Notably, there is no clear signature in these data of the underlying gradient length scale. For example, there is no sigmoidal turnover to a low-h regime and thus no clear

feature indicating the 'range' of the effect. These results indicate that it is likely to be challenging to infer deep physics of the surface gradient by studying $T_g(h)$ data. This is consistent with a previously analytic analysis by Schweizer and Simmons suggesting that it may be functionally implausible to extract detailed information on the form of the gradient, and perhaps even on its range, from mean-film T_g measurements⁸.

Implications for breadth of the relaxation time distribution

While $T_g(h)$ curves thus evidently tend to lack a clear signature of the range of dynamical gradients, our prior work hints³⁶ that superposition of two gradients can have a profound effect on the *distribution* of local relaxation times and $T_g s$ in the ultrathin-film limit. Specifically, gradient superposition effects tend to suppress gradients in very thin freestanding films. This would naturally be expected to alter the breadth of the distribution of relaxation times within the film. Is there some signature of this effect at a whole film level that might provide a promising target for experiment?

The most commonly employed metric for the 'breadth' of the relaxation time spectrum in bulk and thin films is the relaxation stretching exponent β (although there are some complexities with this interpretation 57). This quantity can be obtained from a stretched exponential fit to real-time relaxation data (typically in simulation) or from (for example) a Havrilak-Nagami fit to relaxation spectrum data obtained from frequency-domain methods such as dielectric spectroscopy 58 . How should we expect β to vary with thickness? Could β provide a signature of gradient overlap effects and of the gradient range in whole-film dynamics?

We employ the linear superposition model, together with data for the thick film gradient and the bulk stretching exponent β_{bulk} , to make a prediction for how the stretching exponent should vary with film thickness in films with two (symmetric) dynamically active interfaces. To do so, we describe a layer of material at any distance z from the interface via a stretched exponential relaxation process with a position-dependent relaxation time τ_{KWW} , consistent with the data for relaxation in our films. We employ several simplifying approximations to obtain a tractable calculation. First, we approximate the local stretching exponent as being equal to the bulk value everywhere in the film. This neglects any spatial variation of β, which we expect to be present near the film surface. Indeed, prior work has suggested alterations in dynamic heterogeneity at film surfaces⁵⁹. However, spatial trends in β are extremely difficult to characterize, even in simulation, because any degree of spatial averaging over the gradient in a finite-thickness bin of particles can lead to contamination and erroneous suppression of the measured β value. The assumption of a uniform β thus provides a simple leading-order approximation. Second, we neglect the difference between the KWW fit parameter τ_{KWW} and the relaxation time τ , the latter of which is defined in our study as the time at which $F_s(q,t)$ drops to 0.2. These two timescales are generally similar, but not quite identical, within the range of β values observed in our simulations – we ignore this difference here. Within these approximations, this leads to

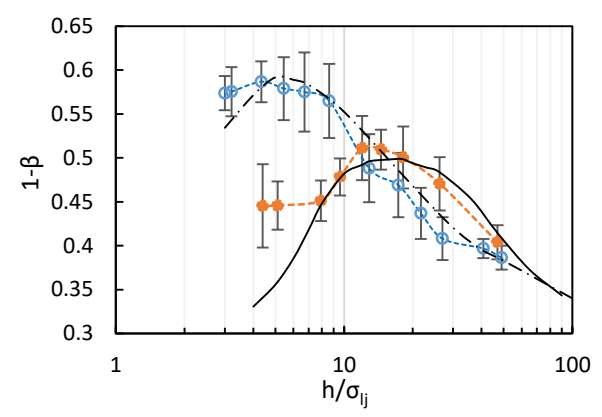


Figure 6. One minus the stretching exponent (measured at low simulation temperatures) vs film thickness for simulated freestanding film (orange circle) and neutrally-supported thin film (open blue circle). The dashed lines are guides to the eye. The black solid line is the prediction of 1- β for a freestanding film based on linear gradient superposition as reflected in equations (10) through (13) and associated discussion in the text. The dot-dashed line is a similar calculation for a supported film with only a single dynamically active interface, as per equation (14).

a prediction for the mean relaxation function $F_s(q,t)$ of a film of thickness h given by

$$\langle F_s(q,t)\rangle = \int_{\tau_{\min}}^{\tau_{\max}} P(\tau) \exp\left[\left(-\frac{t}{\tau}\right)^{\beta_{Bulk}}\right] d\tau$$
 (10)

where $P(\tau)$ is the probability distribution of local mean τ values for layers within the film and τ_{min} and τ_{max} are the lowest and highest values of τ within the film. $P(\tau)$ for a freestanding film can be obtained from

$$\varepsilon(z) = \varepsilon_{0,surf} \exp(-z/\xi_{\Delta F,surf}) + \varepsilon_{0,surf} \exp(-(h - z_{\Delta F,surf})/\xi_{\Delta F,surf})$$
(11)

which specifies the barrier gradient as reflecting a linear superposition of two symmetric decaying exponentials. Combination of equation (11) with equation (5) yields an equation for the relaxation time gradient at a given bulk relaxation time,

$$\tau(T,z) = \tau_B(T) \left(\frac{\tau_B(T)}{\tau^*} \right)^{-\varepsilon_0(h) \left[\exp\left(-z/\xi_{\Lambda F, \text{sury}}\right) + \exp\left(-(h-z)/\xi_{\Lambda F, \text{sury}}\right) \right]}$$
(12)

This equation can be analytically inverted to yield the function $z(\tau)$. We then transform this quantity into a probability distribution function (i.e. the equation for the fraction of the film with a given value of τ) via a change of variables:

$$P(\tau) = \frac{dz/d\tau}{\int_{\tau_{\min}}^{\tau_{\max}} (dz/d\tau) d\tau}$$
 (13)

The resulting function from equation (13) is then substituted into equation (10) to yield a predicted mean-film relaxation function. Both equations (13) and (10) are evaluated numerically. The bounds of the integrals in these equations are given by symmetry for a freestanding film as $\tau_{min} = \tau(z=0)$ and

 $\tau_{\text{max}} = \tau(z=h/2)$. In making this calculation, as noted above, we employ values of ξ and ε_0 measured in the 47 σ_{\square} film. We then fit the resulting predicted $F_s(q,t)$ curve for a film of each thickness h to a stretched exponential, using the same protocol we describe above for the simulation data.

The same approach as that described above is applied for the dynamically neutrally supported film, but in this case equation (11) (for the freestanding film) is replaced with equation (7), which leads to

$$\tau(T,z) = \tau_B(T) \left(\frac{\tau_B(T)}{\tau^*} \right)^{-\varepsilon_0(h) \left[\exp\left(-z/\xi_{\Delta F, surf}\right) \right]}$$
(14)

In place of equation (12). The upper bound of the integrals in equations (13) and (10) then becomes $\tau_{max} = \tau(z=h)$ rather than $\tau_{max} = \tau(z=h/2)$ to reflect the altered symmetry of the film.

The resulting predicted curves of β vs log(h) are shown in Figure 6, where they are compared to simulation data from our prior freestanding film simulations and our new dynamically neutrally supported film simulations. As can be seen here, the prediction of $\beta(h)$ is in excellent agreement with the data for freestanding films down to $^{\sim}8\sigma_{\sqcup}$. For films thinner than $^{\sim}8\sigma_{\sqcup}$, the prediction deviates from the simulated data, as expected due to the elasticity saturation effects previously discussed for ultra-thin freestanding films³⁶. We note that in performing this analysis, we must contend with the empirical temperature dependence of β . We find that β plateaus for low temperatures and is at most weakly temperature dependent for temperature for which the relaxation time of the film $\tau > 10^2 \ \text{for all of our}$ simulations. We thus employ this low-temperature plateau value of β in performing this analysis by taking an average of β over temperatures for which the relaxation time of each film $\boldsymbol{\tau}$ $> 10^2$.

The linear superposition model prediction evidently predicts and explains a nontrivial observed nonmonotonic behaviour observed in freestanding film simulations. This dependence can be understood as follows. For thick films where h > 4.6 ξ , reduction of the film thickness shrinks the bulk-like center region of the film without appreciably impacting the form of the gradients. This leads to a broadening of the relaxation time distribution as the gradient becomes the major component of the film. Once the bulk-like region is gone (around 4.6 ξ), this effect saturates, and the relaxation time distribution breadth plateaus. For appreciably thinner films where the gradients strongly overlap (approximately < 2.3 ξ), the gradient superposition effect causes gradient flattening for simple mathematical reasons associated with addition of two opposed exponential decays. Further reductions in film thickness thus suppress the dynamical gradient, homogenize the film, and narrow the relaxation time distribution.

This non-monotonic behaviour is muted and does not occur until much lower film thicknesses in the neutrally supported film, since no appreciable gradient overlap effects are present to cause gradient flattening at low h. Instead, a reduction in $1-\beta$ only occurs for very thin films such that h is comparable to or

less than ξ . In these extremely thin films, truncation (rather than flattening) of the gradient by the substrate leads to a weak reduction in the overall heterogeneity of dynamics in the film.

If experimentally validated, these findings would indicate that the thickness-variation of the stretching exponent (or other measures of the breadth of the relaxation time distribution) in films with symmetric interfaces could allow for determination of the dynamical gradient range from a mean-film measurement. Specifically, as indicated above, we find the minimum value of β (maximum in 1- β , meaning the most heterogeneous dynamics) is found when the film thickness $h\cong 4-5~\xi.$ Observation of a maximum in the mean-film β for any symmetric film would thus both provide a powerful experimental validation of the proposition that these findings extend to experimental timescales, and potentially allow for extraction of the interfacial dynamic gradient exponential decay range.

Conclusions

A central issue in the study of altered dynamics in nanoscale and nanostructured systems has been the question of whether these systems exhibit genuine 'nanoconfinement' effects – i.e. alterations in dynamics associated with the system's finite size rather than merely with the presence of interfaces. Here we probe this question by studying simulated films supported on a dynamically neutral substrate, possessing a single dynamically active interface, and comparing them to simulated freestanding films possessing two symmetric dynamically active interfaces. Our results indicate that, at least to leading order, no genuine finite size effects are needed to explain and predict the behaviour of simulated bead-spring films of finite thickness on the timescales accessible to simulation, either in the case of freestanding films or a supported film. Crucially, we find that in the presence of one dynamically active interface and one dynamically neutral interface, the system behaviour can be predicted based purely on the single gradient emanating from the dynamically active interface, with a truncation plane at the neutral interface. This finding holds to an excellent approximation down to films as thin as three segmental layers thick.

A key feature of this work is the use of a nearly dynamically neutral substrate, which imposes little to no gradient in dynamics on nearby material. This state is achieved simply by tuning the polymer/substrate interaction to a level yielding dynamic neutrality. Crucially, a true finite size effect would by definition be insensitive to this type of surface interaction. The absence of such an effect in the presence of a dynamically neutral substrate thus implies a lack of finite size effects more generally, at least in the timescale and molecular weight ranges accessible to these simulations. Moreover, because of the absence of a dynamical gradient at the substrate, any finite size effect would be quite easy to detect within this model if it were in fact present.

While the present findings obtain within the bead-spring polymer system studied here, several prior perspectives authored or co-authored by one of us have identified a remarkable degree of near-universality of these interfacial gradient effects in simulated systems, spanning multiple model systems, multiple interfaces, and multiple geometries^{8,10}. We believe that this degree of transferability of behaviour across numerous simulated systems suggests that the bead-spring polymer system studied here likely provides a generalizable model for the core physics governing these interfacial effects on simulation timescales. We thus expect our conclusions to obtain for a wide range of systems studied on these timescales.

From a physical standpoint, we note that the behaviour of the single-interface gradients that evidently dominate these films' properties even down to the 3-4 segmental layer range has previously been predicted, without adjustable parameters, by the Elastically Cooperative Nonlinear Langevin Equation Theory of glass formation⁵⁵. Within that theory, these gradients are driven by a combination of alterations in caging scale, which propagate into the film over a medium range, and interfacial truncation and alteration of a scale-free elastic activation field, which impacts dynamics over a long range from the interface. The present findings thus add more weight to growing evidence that the ECNLE theory is predictive of the features of translational dynamics in low- to moderate-molecular-weight polymer thin films on the timescales accessible to simulation.

Finally, our results s a new potential experimental target that could provide additional validating evidence for the proposition that the gradient behaviour observed in these and other simulations extends to experimental timescale. In particular, we find that the breadth of the mean-film relaxation process, as measured by the mean-film stretching exponent β , should exhibit a maximum in freestanding films for film thickness in the range of 4-5 times the surface gradient range. This effect is expected to also be present in films supported on highly unattractive substrates that induce a local enhancement in dynamics. Direct measurement of this maximum would validate this simulation prediction, which emerges fundamentally from the finding that thin-film behaviour is dominated by exponential gradient superposition effects, and that exponential gradient superposition in turn leads to gradient flattening and thus a less dynamically heterogeneous film. We note that a weaker nonmonotonicity is observed even for a film supported on a dynamically neutral substrate, but this effect is shifted to much thinner films of order the gradient range itself – a consequence of mere truncation of the gradient by the substrate. Even here, this maximum would provide evidence that gradients do not innately grow sharper in thinner films but are rather subject to interfacial truncation.

If this prediction is experimentally validated, such measurements could additionally allow extraction of the fundamental surface range of dynamical gradients from *mean-film* measurements. Since the maximum in β in a freestanding film is in the range of 4-5 the exponential decay range, observation of this maximum could allow a fairly narrow

determination of the surface gradient range from freestanding film measurements. One possible route to do so would be via dielectric spectroscopy measurements of thin films, although this would require careful treatment of such nontrivial issues as the manner in which the measurements weight with depth (which can be highly measurement-dependent⁴¹) and the treatment of the depth dependence as reflecting parallel⁶⁰ or serial⁶¹ capacitors depending on the sample geometry. Such measurements, if these complexities could be resolved, could complement and broaden insights from recent surface diffusion measurements in a series of small molecules, which suggested a gradient range consistent with these simulations²⁷. Confirmation of this correspondence via experimental measurements of relaxation breadth in thinner films could thus present the opportunity to more strongly unify computational experimental findings on "nanoconfinement" effects on dynamics from over 30 years of research.

Author Contributions

AG performed the simulations; both authors contributed to research conceptualization, data analysis, and manuscript preparation.

Conflicts of interest

There are no conflicts to declare.

Acknowledgements

This material was based upon work supported by the National Science Foundation under Grant No. CBET - 2208238. The authors acknowledge helpful discussions with Dr. Ahn Phan and Dr. Kenneth Schweizer.

Notes and references

- 1 J. A. Forrest and K. Dalnoki-Veress, *Advances in Colloid and Interface Science*, 2001, **94**, 167–195.
- 2 M. Alcoutlabi and G. B. McKenna, *Journal of Physics:* Condensed Matter, 2005, **17**, R461–R524.
- 3 J. Baschnagel and F. Varnik, J. Phys.: Condens. Matter, 2005, 17, R851.
- 4 C. B. Roth and J. R. Dutcher, *Journal of Electroanalytical Chemistry*, 2005, **584**, 13–22.
- 5 G. B. McKenna, *The European Physical Journal Special Topics*, 2010, **189**, 285–302.
- 6 R. Richert, Annual Review of Physical Chemistry, 2011, **62**, 65–84
- 7 M. D. Ediger and J. A. Forrest, *Macromolecules*, 2014, **47**, 471–478.
- 8 K. S. Schweizer and D. S. Simmons, *Journal of Chemical Physics*, 2019, **151**, 240901.
- 9 C. B. Roth, *Chemical Society Reviews*, 2021, **50**, 8050–8066.

- 10 D. S. Simmons, Macromol. Chem. Phys., 2016, 217, 137-148.
- 11 J. L. Keddie, R. A. L. Jones and R. A. Cory, *Europhysics Letters*, 1994, **27**, 59–64.
- 12 C. L. Jackson and G. B. McKenna, *Chemistry of Materials*, 1996, **8**, 2128–2137.
- 13 J. H. van Zanten, W. E. Wallace and W. Wu, *Physical Review E*, 1996, **53**, R2053–R2056.
- 14 D. J. Pochan, E. K. Lin, S. K. Satija and W. Wu, *Macromolecules*, 2001, **34**, 3041–3045.
- 15 T. Kajiyama, K. Tanaka and A. Takahara, *Macromolecules*, 1997, **30**, 280–285.
- 16 D. S. Fryer, R. D. Peters, E. J. Kim, J. E. Tomaszewski, J. J. de Pablo, P. F. Nealey, C. C. White and W. Wu, *Macromolecules*, 2001, **34**, 5627–5634.
- 17 C. J. Ellison and J. M. Torkelson, *Nature Materials*, 2003, **2**, 695–700.
- 18 Y. Guo, C. Zhang, C. Lai, R. D. Priestley, M. D'Acunzi and G. Fytas, *ACS Nano*, 2011, **5**, 5365–5373.
- 19 C. Zhang, Y. Guo and R. D. Priestley, *Macromolecules*, 2011, **44**, 4001–4006.
- 20 R. J. Lang, W. L. Merling and D. S. Simmons, *ACS Macro Lett.*, 2014, **3**, 758–762.
- 21 P. Z. Hanakata, B. A. P. Betancourt, J. F. Douglas and F. W. Starr, *The Journal of Chemical Physics*, 2015, **142**, 234907.
- 22 D. Diaz-Vela, J.-H. Hung and D. S. Simmons, *ACS Macro Lett.*, 2018, **7**, 1295–1301.
- 23 A. Shavit and R. A. Riggleman, *J. Phys. Chem. B*, 2014, **118**, 9096–9103.
- 24 S. Peter, H. Meyer and J. Baschnagel, *Journal of Polymer Science Part B: Polymer Physics*, 2006, **44**, 2951–2967.
- 25 Y. Zhou and S. T. Milner, *Macromolecules*, 2017, **50**, 5599–5610.
- 26 P. Scheidler, W. Kob and K. Binder, *Europhysics Letters (EPL)*, 2002, **59**, 701–707.
- 27 Y. Li, W. Zhang, C. Bishop, C. Huang, M. D. Ediger and L. Yu, *Soft Matter*, 2020, **16**, 5062–5070.
- 28 Y. Li, A. Annamareddy, D. Morgan, Z. Yu, B. Wang, C. Cao, J. H. Perepezko, M. D. Ediger, P. M. Voyles and L. Yu, *Phys. Rev. Lett.*, 2022, **128**, 075501.
- 29 Paul Z. Hanakata, Jack F. Douglas, and Francis W. Starr, *Journal of Chemical Physics*, 2012, **137**, 244901.
- 30 J. H. Mangalara, M. D. Marvin, N. R. Wiener, M. E. Mackura and D. S. Simmons, *The Journal of Chemical Physics*, 2017, **146**, 104902.
- 31 D. D. Hsu, W. Xia, J. Song and S. Keten, *MRS Communications*, 2017, **7**, 832–839.
- 32 A. Ghanekarade, A. D. Phan, K. S. Schweizer and D. S. Simmons, *Nat. Phys.*, 2023, **19**, 800–806.
- 33 R. P. White and J. E. G. Lipson, *Phys. Rev. Lett.*, 2020, **125**, 058002.
- 34 W. Heinrich and B. Stoll, *Colloid & Polymer Sci*, 1985, **263**, 873–878.

- 35 D. Vela, A. Ghanekarade and D. S. Simmons, *Macromolecules*, 2020, **53**, 4158–4171.
- 36 A. Ghanekarade, A. D. Phan, K. S. Schweizer and D. S. Simmons, *PNAS*, 2021, **118**, e2104398118.
- 37 Y. Zhang, E. C. Glor, M. Li, T. Liu, K. Wahid, W. Zhang, R. A. Riggleman and Z. Fakhraai, *J. Chem. Phys.*, 2016, **145**, 114502.
- 38 Y. Zhang, C. N. Woods, M. Alvarez, Y. Jin, R. A. Riggleman and Z. Fakhraai, *J. Chem. Phys.*, 2018, **149**, 184902.
- 39 K. Kremer and G. S. Grest, *The Journal of Chemical Physics*, 1990, **92**, 5057–5086.
- 40 M. E. Mackura and D. S. Simmons, *J. Polym. Sci. Part B: Polym. Phys.*, 2014, **52**, 134–140.
- 41 J. H. Mangalara, M. E. Mackura, M. D. Marvin and D. S. Simmons, *The Journal of Chemical Physics*, 2017, **146**, 203316.
- 42 S. Plimpton, *Journal of Computational Physics*, 1995, **117**, 1–19.
- 43 J.-H. Hung, T. K. Patra, V. Meenakshisundaram, J. H. Mangalara and D. S. Simmons, *Soft Matter*, 2018, **15**, 1223–1242.
- 44 M. Z. Slimani, A. J. Moreno and J. Colmenero, *Macromolecules*, 2011, **44**, 6952–6961.
- 45 B. A. P. Betancourt, J. F. Douglas and F. W. Starr, *Soft Matter*, 2012, **9**, 241–254.
- 46 R. J. Lang and D. S. Simmons, *Macromolecules*, 2013, **46**, 9818–9825.
- 47 G. Williams and D. C. Watts, *Trans. Faraday Soc.*, 1970, **66**, 80–85.
- 48 F. Kohlrausch, Pogg. Ann. Physik, 1863, 119, 352.
- 49 J.-H. Hung, J. H. Mangalara and D. S. Simmons, *Macromolecules*, 2018, **51**, 2887–2898.
- 50 J. H. Mangalara and D. S. Simmons, *ACS Macro Lett.*, 2015, **4**, 1134–1138.
- 51 H. Vogel, Phys. Zeit., 1921, 22, 645-646.
- 52 G. S. Fulcher, *Journal of the American Ceramic Society*, 1925, **8**, 339–355.
- 53 W. L. Merling, J. B. Mileski, J. F. Douglas and D. S. Simmons, *Macromolecules*, 2016, **49**, 7597–7604.
- 54 T. Rahman and D. S. Simmons, *Macromolecules*, 2021, **54**, 5935–5949.
- 55 A. D. Phan and K. S. Schweizer, *Macromolecules*, 2019, **52**, 5192–5206.
- 56 P. A. O'Connell, J. Wang, T. A. Ishola and G. B. McKenna, *Macromolecules*, 2012, **45**, 2453–2459.
- 57 D. Diaz Vela and D. S. Simmons, *J. Chem. Phys.*, 2020, **153**, 234503.
- 58 F. Kremer and A. Schönhals, *Broadband Dielectric Spectroscopy*, Springer Science & Business Media, 2012.
- 59 R. J. S. Ivancic and R. A. Riggleman, *PNAS*, 2020, **117**, 25407–25413.
- 60 C. Rotella, S. Napolitano and M. Wübbenhorst, *Macromolecules*, 2009, **42**, 1415–1417.
- 61 A. Serghei, M. Tress and F. Kremer, *The Journal of Chemical Physics*, 2009, **131**, 154904.

62 W. Kob, S. Roldán-Vargas and L. Berthier, *Nature Phys*, 2012, **8**, 164–167.